Plant, Cell & Environment

Plant, Cell and Environment (2016) **39**, 1835–1847 doi: 10.1111/pce.12749

Original Article

Element distribution and iron speciation in mature wheat grains (*Triticum aestivum* L.) using synchrotron X-ray fluorescence microscopy mapping and X-ray absorption near-edge structure (XANES) imaging

Niels De Brier[1], Sara V. Gomand[1], Erica Donner[2], David Paterson[3], Erik Smolders[4], Jan A. Delcour[1] & Enzo Lombi[2]

[1]Laboratory of Food Chemistry and Biochemistry, Leuven Food Science and Nutrition Research Centre (LFoRCe), KU Leuven, Leuven B-3001, Belgium, [2]Centre for Environmental Risk Assessment and Remediation, University of South Australia, Mawson Lakes, South Australia 5095, Australia, [3]Australian Synchrotron, Clayton, Victoria 3168, Australia and [4]Division of Soil and Water Management, KU Leuven, Leuven B-3001, Belgium

ABSTRACT

Several studies have suggested that the majority of iron (Fe) and zinc (Zn) in wheat grains are associated with phytate, but a nuanced approach to unravel important tissue-level variation in element speciation within the grain is lacking. Here, we present spatially resolved Fe-speciation data obtained directly from different grain tissues using the newly developed synchrotron-based technique of X-ray absorption near-edge spectroscopy imaging, coupling this with high-definition μ-X-ray fluorescence microscopy to map the co-localization of essential elements. In the aleurone, phosphorus (P) is co-localized with Fe and Zn, and X-ray absorption near-edge structure imaging confirmed that Fe is chelated by phytate in this tissue layer. In the crease tissues, Zn is also positively related to P distribution, albeit less so than in the aleurone. Speciation analysis suggests that Fe is bound to nicotianamine rather than phytate in the nucellar projection, and that more complex Fe structures may also be present. In the embryo, high Zn concentrations are present in the root and shoot primordium, co-occurring with sulfur and presumably bound to thiol groups. Overall, Fe is mainly concentrated in the scutellum and co-localized with P. This high resolution imaging and speciation analysis reveals the complexity of the physiological processes responsible for element accumulation and bioaccessibility.

Key-words: Aleurone; crease region; embryo; nutrient elements.

INTRODUCTION

Iron (Fe) deficiency is the most common and widespread nutritional disorder in the world. It affects a large number of children and women in developing countries but is also prevalent in Western countries. Globally, anaemia affects 1.6 billion people, and thus about 25% of the world's population [World Health Organization (WHO), 2008, 2015]. WHO lists the 50% reduction of anaemia in women of reproductive age as one of the most important global targets for 2025 (www.who.org). Zinc (Zn) deficiency causes a variety of disorders such as impaired immune function, increased morbidity from diarrhoea, pneumonia and child stunting (Brown *et al.* 2009; Prasad 2009). An estimated 17% of the world's population risk inadequate zinc intake (Wessells & Brown 2012).

As a staple food, wheat plays a particularly important role in daily energy supply. It accounts for more than 25% of the caloric intake in developing countries and an estimated intake of as much as 50% in West Asian countries (Cakmak 2008). As such, it also is one of the major pathways through which humans acquire nutrient elements like Fe and Zn. Nevertheless, cereal-based diets supply only about 0.7–1.4 mg Fe daily and are insufficient to meet Fe requirements in women and many men (Baynes & Bothwell 1990). Therefore, it has been suggested that, in developing countries, biofortification strategies would focus on the staple foods that dominate people's diet (Graham *et al.* 2007; Pfeiffer & McClafferty 2007).

From the outside to the inside, wheat grains consist of the pericarp, the seed coat (testa), the nucellar epidermis, the aleurone layer and the starchy endosperm (Fig. 1). The embryo is located on the dorsal side of the wheat grain. The elongated pericarp cells (80–300 μm long and 12–50 μm wide) make up about 4–6% of the wheat grain, are devoid of cytoplasm at maturity and have lignified cell walls (Bradbury *et al.* 1956b; Bechtel *et al.* 2009). The pericarp is a multilayered tissue and from the outside to the inside comprises the epidermis, the hypodermis, the intermediate cells, the cross cells and the tube cells (Bradbury *et al.* 1956b; Bechtel *et al.* 2009). The seed coat (testa) makes up about 0.5 to 0.7% of the wheat grain by weight (Shetlar *et al.* 1947). It consists of three layers: a thick outer cuticle, a colour layer (pigment strand) and a thin inner cuticle (Bechtel *et al.* 2009; Delcour & Hoseney 2010). The nucellar epidermis, also called hyaline layer, is situated between the aleurone layer and the seed coat and accounts for about 1.4% of the wheat grain (Shetlar *et al.* 1947). The aleurone,

Correspondence: N. De Brier. Fax: +32 16 321997; e-mail: niels.debrier@biw.kuleuven.be

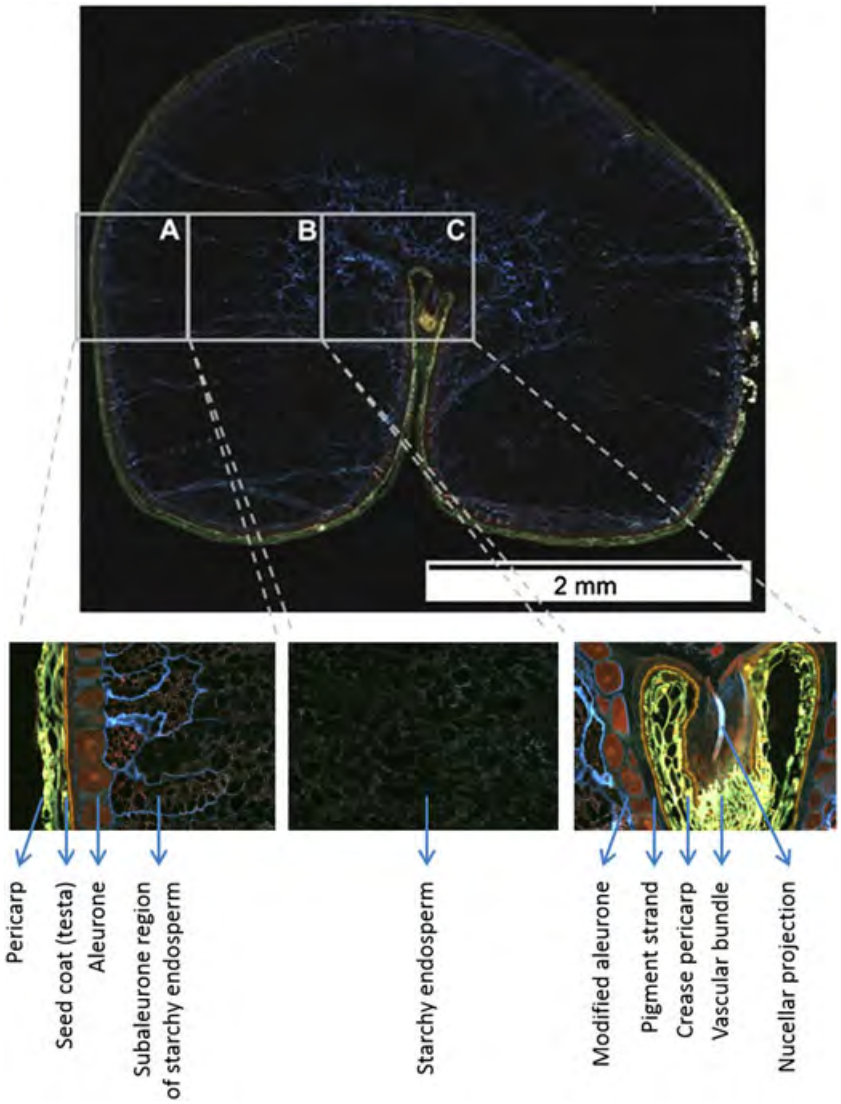

Figure 1. Section of a wheat grain bisected transversely in a central plane stained with acid fuchsin–calcofluor showing the cellular structure of different tissues within the (A) aleurone layer, (B) starchy endosperm and (C) crease region. Proteins appear red, cell walls rich in β-glucan appear light blue, and lignified cell walls of the seed coat appear yellowish brown (adapted from Dornez *et al.* 2011 with permission from Elsevier).

which represents 5–8% of the wheat grain mass, consists of a single layer of living cubic cells (37–65 μm by 25–75 μm) containing vacuoles (granular globoids) filled with reserves (Tanaka *et al.* 1974; Morrison *et al.* 1975; Barron *et al.* 2007; Bechtel *et al.* 2009; Brouns *et al.* 2012; Moore *et al.* 2012). Essentially, mature starchy endosperm is the largest tissue of wheat grains (about 80 to 85%). The starchy endosperm cells contain starch granules, which are embedded in a continuous protein matrix (Bradbury *et al.* 1956c; Delcour & Hoseney 2010). The embryo consists of two main parts: the scutellum, which functions as storage organ, and the embryonic axis, which contains the shoot and root primordia and develops into the seedling during germination. The scutellum and embryonic axis each make up about 1.5% on average of the dry matter of the wheat grain (Dubois *et al.* 1960; Barron *et al.* 2007). The scutellum lies between the embryonic axis and the starchy endosperm (Bradbury *et al.* 1956a; Evers & Millar 2002; Bechtel *et al.* 2009).

During wheat grain maturation, most nutrient elements are transported mainly via the phloem. They pass into the grain through specialized cells in the crease region (Borg *et al.* 2009; White 2012). Elements like calcium (Ca) and manganese (Mn) have low mobility in the phloem (White 2012). They enter the grain through the vascular system of the pericarp, which may have a direct xylem supply. It is equally possible that they reach the pericarp vasculature through the phloem as a result of xylem discontinuity in the grain stalk (O'Brien *et al.* 1985; Pearson *et al.* 1995; White 2012). Nutrient elements reach the nucellar projection by crossing the crease vascular parenchyma and the pigment strand (Fig. 1). The nucellar projection originates from the same tissue as the nucellar epidermis in the outer kernel layers (Bechtel *et al.* 2009; Dornez *et al.* 2011). Next, the elements move from the nucellar projection to the apoplast through the vascular bundle (transfer cells). From here, they are taken up by the modified aleurone cells (Fig. 1) and distributed to the aleurone layer, the starchy

endosperm and the embryo (Borg *et al*. 2009; Tauris *et al*. 2009). However, an in-depth understanding of element transport and accumulation in wheat grains is still lacking.

Most wheat for human consumption is roller milled to produce white flour (starchy endosperm) with simultaneous removal of the embryo and the bran (including the pericarp, seed coat, nucellar epidermis and aleurone) (Delcour & Hoseney 2010). The starchy endosperm is relatively poor in micronutrients. These are much more abundant throughout the bran and germ tissues of the wheat grain (Liu *et al*. 2008; Tang *et al*. 2008; Delcour & Hoseney 2010; De Brier *et al*. 2015). However, in the aleurone, elements such as Fe, Zn, Ca, Mn, magnesium and copper (Cu) occur as phytates, the main storage form of phosphorus (P) in cereal grains (Jacobsen & Slotfeldt-Ellingsen 1983; Lott *et al*. 1985; Eeckhout & De Paepe 1994; De Brier *et al*. 2015). As a result, the nutrient elements in the bran have low bioaccessibility and, hence, are poorly available for intestinal uptake by humans (Lopez *et al*. 2002). The phytates are present as granules embedded in protein-rich globoid structures (Moore *et al*. 2012).

For nutrient elements, concentration, speciation and spatial distribution are important. Concentrations and speciation vary with the wheat tissue examined. Recently, size-exclusion chromatography, coupled with inductively coupled plasma mass spectrometry, has been used to determine the speciation of Fe and Zn in barley embryo (*Hordeum vulgare* L.) (Persson *et al*. 2009), rice flour (Lee *et al*. 2011) and wheat (flour and whole meal) (Eagling *et al*. 2014; Xue *et al*. 2014). Eagling *et al*. (2014) found that 85% of the extractable Fe and Zn in wheat flour is bound to nicotianamine (NA)/deoxymugineic acid. However, this technique provides no information on the speciation of Fe and Zn at tissue level. In contrast, synchrotron-based techniques are powerful for unravelling element distribution and speciation patterns in biological samples without the need of extractions, even including *in vivo* studies (Weekley *et al*. 2013). X-ray fluorescence microscopy (XFM) is used for element distribution imaging, whilst laterally resolved X-ray absorption near-edge structure spectroscopy (μ-XANES or XANES imaging) can be used to investigate element distribution and speciation. μ-XFM allows high-definition mapping of elements of whole grain sections with high lateral resolution without losing elemental detection (Lombi *et al*. 2009; Takahashi *et al*. 2009; Lombi *et al*. 2011c; De Brier *et al*. 2015). However, in spite of the importance of wheat as a staple food, only a few studies have mapped the distribution of elements in wheat grains and/or determined their speciation. Singh *et al*. (2013) reported the distribution pattern of Fe by XFM and μ-particle-induced X-ray emission and its speciation by XANES in whole wheat grains. They found evidence for the presence of oxygen, P and sulfur (S) in the local chemical environment of Fe in wheat grains. However, they did not yield element distribution information at the tissue level. Singh *et al*. (2014) subsequently performed micro-imaging of nutrient elements in the different tissues of wheat grains, but the Fe speciation was only inferred from co-localization with P. Neal *et al*. (2013) focused on the chelation of Zn and Fe with phytate in wild-type and ferritin-expressing wheat grains, and although they found Fe phytate in ferritin-expressing wheat grains, there was also evidence of a structure lacking P.

The spatial differences in Fe-speciation within wheat grains are still not completely unravelled. In the present study, the associations of micronutrient elements with their possible ligands (P and S) in nutrient-dense regions such as the aleurone, crease and embryo were investigated by high-definition lateral resolution element imaging using deliberate over-sampling to enhance lateral resolution. The speciation of Fe was not only determined from the co-localization results, it was also investigated directly using the newly available method of XANES imaging (Etschmann *et al*. 2014). The spatially resolved XANES imaging analyses focused on the aleurone cells, the main storage tissue of nutrient elements and the crease region, which is of importance regarding element transport. Together, this information on the distribution of Fe and its possible ligands and the structural identification and spatial distribution of Fe species paves the way to a better understanding of the physiological processes responsible for Fe accumulation in wheat grains and to allow more targeted biotechnology approaches to improve the nutrient status of crop plants. The further development of biofortified wheat will lead to a more sustainable way of increasing nutrient intake than supplementation. Increasing the Zn and Fe concentrations of wheat grains can reasonably be expected to improve human health and is an important global challenge. These findings may also shed light on micronutrient bioaccessibility in processed wheat.

MATERIALS AND METHODS

Materials

Wheat grains (cv. Akteur, harvest 2012, E-type winter wheat exhibiting excellent bread making properties, moisture content 14.8%) were supplied by Dossche Mills (Deinze, Belgium). The concentrations of P, Fe, Zn, Cu and Mn in intact wheat grains were determined in six replicates by digesting accurately weighed samples (0.1 g) with 2.00 mL of ultrapure HNO_3 for 4 h followed by dilution to 10.0 mL of Milli-Q water (18.2 U; Milli-Q Plus, Merck Millipore, Darmstadt, Germany). Target elements were subsequently analysed by inductively coupled plasma mass spectrometry (Agilent 7700x, Santa Clara, CA, USA). A reference wheat flour sample with certified element composition was included: NIST1567 Wheat (National Institute of Standards and Technology, Gaithersburg, MD, USA). All elements reported were recovered within 10% of the certified values. The total concentrations, in mg of the element/kg dry matter (±standard deviation, $n = 6$), were 3800 ± 160 (P), 37 ± 2 (Fe), 30 ± 3 (Mn), 25 ± 2 (Zn) and 3.8 ± 0.3 (Cu). The overall concentrations are similar to the concentrations detected at X-ray fluorescence microscopy at Australian Synchrotron in rice (Lombi *et al*. 2009) and barley (Lombi *et al*. 2011c).

Imaging of element distribution

Longitudinal and transverse cross sections (80 μm thick) of the middle part of the wheat grains were made using the technique described in Lombi *et al.* (2009). Briefly, the wheat grains were glued to a plastic support and sliced using a vibrating diamond blade (GFD Gesellschaft für Diamantprodukte, Ulm, Germany) microtome to obtain a flat surface (Microm HM 650 Vibratome, Thermo Scientific, Walldorf, Germany). A piece of Kapton polyimide film was then pressed on the surface of the residual grain, with the diamond blade of the microtome cutting underneath. In this way, sections were directly obtained on the Kapton tape without the need for embedding. The use of thin sections is necessary to reduce the distortion of the elemental maps caused by the penetrating nature of the X-rays, as the output is translated into a 2D compression of the illuminated sample volume (Lombi *et al.* 2011b).

Elemental X-ray fluorescence maps were collected using the XFM undulator beamline at the Australian Synchrotron (Paterson *et al.* 2011). Laterally resolved elemental maps were collected using the XFM beamline equipped with a Si(111) monochromator and Kirkpatrick–Baez mirrors focusing the beam to a spot size of approximately 3 × 2 μm (horizontal × vertical). An incident beam energy of 10 keV was used, and the X-ray fluorescence (XRF) signal was collected using a 384-element Maia detector system which collects a full XRF spectrum for each image pixel. The samples were analysed continuously on-the-fly in the horizontal direction with pixels of 4.0 μm (transverse cross sections), 2.0 μm (longitudinal embryo section) or 0.4 μm (very high resolution maps through deliberate oversampling). The pixel (4.0 μm, 2.0 μm or 0.4 μm) transit time was approximately 5.20 ms, 2.60 ms or 0.52 ms, respectively. The full XRF spectra were then analysed using GEOPIXE (Ryan 2000). This software uses dynamic analysis to subtract the background fluorescence signal and resolves overlapping peaks to generate element concentration maps. Using this technique, the concentration distributions of K, Ca, Fe, Zn, Cu and Mn were mapped. Using the X-ray cross section of Ebel *et al.* (2003), the fundamental parameter database of Elam *et al.* (2002) extended with the particle-induced X-ray emission data (Ryan *et al.* 2005), and corrections for self-absorption, absorption in air and the efficiency response of the detector obtained using standard metal (Mn, Pt) foils, semi-quantitative values for the different elements, were calculated. In total, we analysed eight cross sections and three longitudinal sections originating from 11 independently sectioned wheat grains. We here show representative results of high-quality cross and longitudinal sections.

As the earlier version of the Maia detector used in this study cannot detect lower than 4 keV or elements lighter than potassium (K) we used a Vortex-EM detector (Hitachi High-Technologies Science America, Inc., Los Angeles, CA, USA) to collect the fluorescence signal of elements such as P and S. Small rectangular areas were mapped at the regions of interest using an incident energy of 10 keV and placing the Vortex detector orthogonally to the incident beam. To avoid self-absorption artefacts, especially in the case of P, the boundary of the grain furthest from the detector was scanned so that the amount of grain material between the volume illuminated by the beam and the detector was constant. The elemental maps were collected using a dwell time per pixel of 1 s and step sizes of 1 and 2 μm in the vertical and horizontal directions, respectively. The dwell time for the Vortex detector is substantially larger than for the Maia. Furthermore, the sensitivity of X-ray fluorescence mapping drops rapidly with decreasing atomic number; therefore, increased integration times are required when measuring light elements such as P. Therefore, only two regions were selected from one representative cross section and one region from one representative longitudinal section. Elemental distributions were refined by fitting the fluorescence spectrum obtained at each location using the MAPS package (Stefan Vogt, Advanced Photon Source, Chicago, USA).

Fe X-ray absorption near-edge structure imaging

X-ray absorption near-edge structure imaging is a recently developed technique that decreases the risk of beam damage during speciation analysis (Lombi *et al.* 2011a; Etschmann *et al.* 2014). In essence, a highly sensitive fluorescence detector is used to rapidly collect 'stacks' of XRF maps, from which a XANES spectrum can potentially be extracted for each and every pixel. To date, this technique has only been used in plant science to investigate As and Se speciation in roots at toxic concentrations (Kopittke *et al.* 2014; Wang *et al.* 2015), and to the best of our knowledge, this is the first time that XANES imaging has been used to investigate the speciation of an essential element in edible grains. In this study, laterally resolved XANES stacks were obtained by scanning the entire area of interest 89 times whilst progressively decreasing the incident X-ray energy from 7370 to 7062 eV across the Fe K-edge. Two different areas of interest from one representative cross section were scanned. This approach has the advantage, in comparison to 'point' or μ-XANES, of providing comprehensive speciation distribution data whilst minimizing operator bias, as the selection of individual points of interest for spectral analysis is not required. The very high sensitivity of the Maia detector also greatly decreases the residence time of the beam at each pixel (i.e. 348 ms/pixel for XANES imaging in this study versus a typical 20 min acquisition time for μ-XANES). This latter aspect is important in terms of reducing the risk of beam damage; this is a particularly significant issue in case of redox sensitive elements such as Fe. The GEOPIXE 'energy association' module was used to identify and select areas for XANES imaging. Specifically, pixel populations were selected where the speciation varied and the concentration ratios between two energies for each pixel were compared. The XANES spectra were extracted from pixels within the selected areas in the stack series and subsequently background and baseline corrected using ATHENA v. 0.8.061 (Ravel & Newville 2005). For these data, linear

combination fitting (LCF) was performed, and the combination of standards yielding the lowest residual parameter was chosen as the most likely set of components. The weighting factors were constrained between 0 and 1, and the combined species weightings were forced to sum to 1. In the case of the LCF method, the R-factor and reduced chi-square obtained are statistical parameters for the goodness of the fit. The R-factors are 0.000673, 0.000677 and 0.001970, and the reduced chi-squares are 0.0005457, 0.000518 and 0.0015660 for the aleurone, nucellar projection and modified aleurone, respectively. The LCF approach is not free from uncertainties and limitations. Its correctness is affected by the choice of standards that are used in the fitting procedure; in addition, minor species present (e.g. representing <10% of the total) should be considered with caution (Grafe *et al*. 2014). The following standards were used in the fitting procedure: sulfate Fe^{2+}, NA Fe^{2+}, phytate Fe^{2+}, cysteine Fe^{2+}, citrate Fe^{2+}, phytate Fe^{3+}, NA Fe^{3+}, cysteine Fe^{3+}, citrate Fe^{2+}, ferritin Fe^{3+} and FeO(OH). The standards were prepared in a N_2-filled anaerobic chamber using degassed water. Ferrous and ferric solutions were mixed with the various ligands (in a molar ratio of 1:1.1), and the pH was adjusted to 6 to ensure complete complexation of the Fe. Thin strips of filter paper were then dipped into the solutions to absorb the standard compounds/complexes. These paper strips were then wrapped in 4 µm ultralene film to protect them from oxygen and scanned as described in the preceding texts.

RESULTS AND DISCUSSION

X-ray fluorescence microscopy of elements in wheat grains

In wheat grains, nutrient elements are not homogeneously distributed (Mazzolini *et al*. 1985; Liu *et al*. 2008; Neal *et al*. 2013; Singh *et al*. 2013; Singh *et al*. 2014). Large gradients in their distribution exist between and within the different tissues. The aleurone, the crease region and the embryo are particularly micronutrient dense (Figs. 2 and 5). Compared with these tissues, there is a much less Fe and Zn in the outer bran tissues and starchy endosperm (Figs. 2 and 5). Hence, the distributions of these elements within the aleurone,

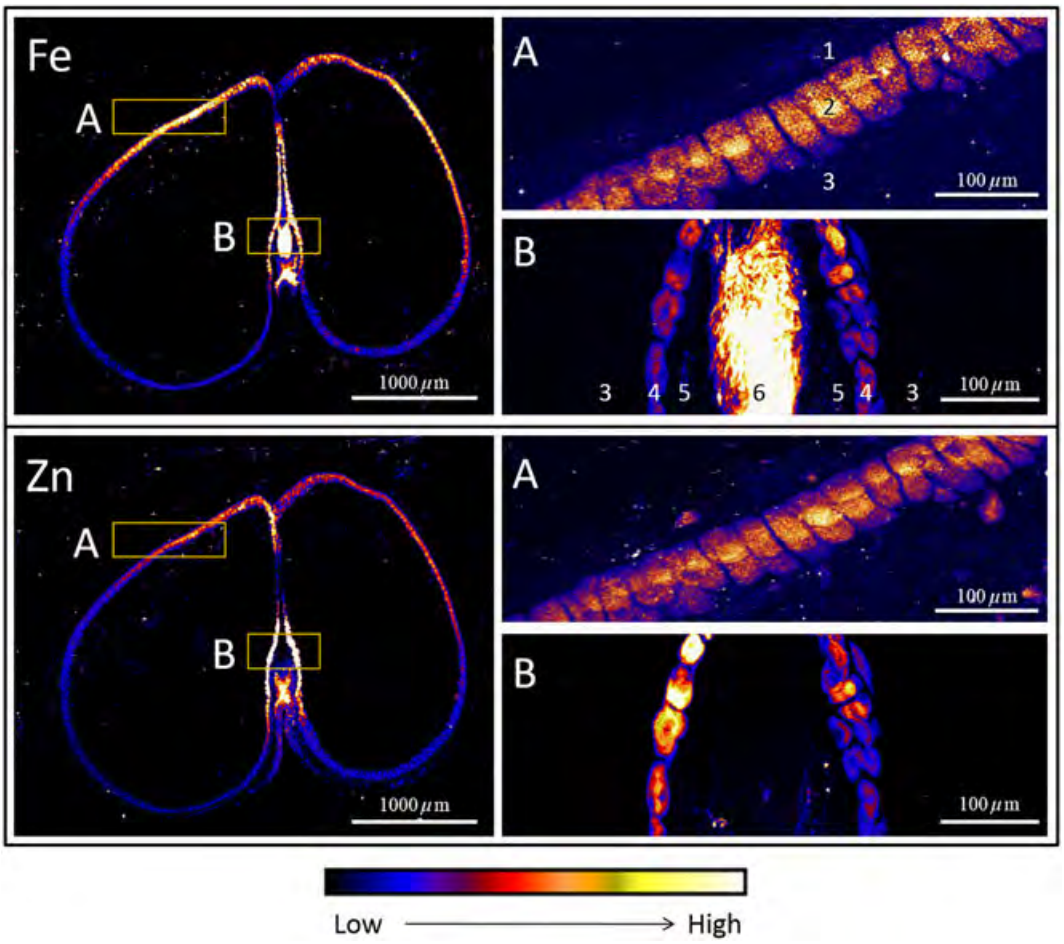

Figure 2. Elemental maps of a wheat grain bisected transversely in a central plane (1, pericarp; 2, aleurone; 3, starchy endosperm; 4, modified aleurone cells; 5, pigment strand and 6, nucellar projection) with a lateral resolution of 4 × 4 µm and (A) a detail picture of the individual aleurone cells and (B) crease region with very high lateral resolution (pixel size of 0.4 × 0.4 µm by oversampling). The color scale represents different concentrations, with black and white corresponding to the lowest and highest concentration, respectively.

crease region and embryo tissues were investigated in detail. The overall concentrations of Fe and Zn (cf. supra) are in line with earlier published concentrations (17 to 75 mg Fe/kg and 5 to 46 mg Zn/kg; Rengel *et al*. 1999; Piironen *et al*. 2009; Cakmak *et al*. 2010).

Aleurone

Figures 2 and S1 show the distributions of Fe and Zn in a mature wheat grain cross section obtained using XFM. Individual aleurone cells can be clearly distinguished in the elemental maps. The very high-resolution XFM images of the aleurone (Fig. 2A) reveal the spherical phytate globoids to which Fe and Zn are confined.

In wheat, most of the nutrient elements are chelated to phytate, which make them unavailable for intestinal uptake by humans and monogastric animals (Lopez *et al.* 2002). To gain more insight into their chemical speciation, the spatial associations of Fe, Mn, Cu and Zn with their possible ligands P (phytate; Eeckhout & De Paepe 1994) and S (cysteine and especially methionine; Li *et al.* 2010) were examined. Figure 3B shows line scans across the bran tissues of mature wheat grains, representing the average concentrations of the vertical areas indicated by the box in the elemental map (Figs. 3A and S2). P distribution is highly localized to a region ranging between

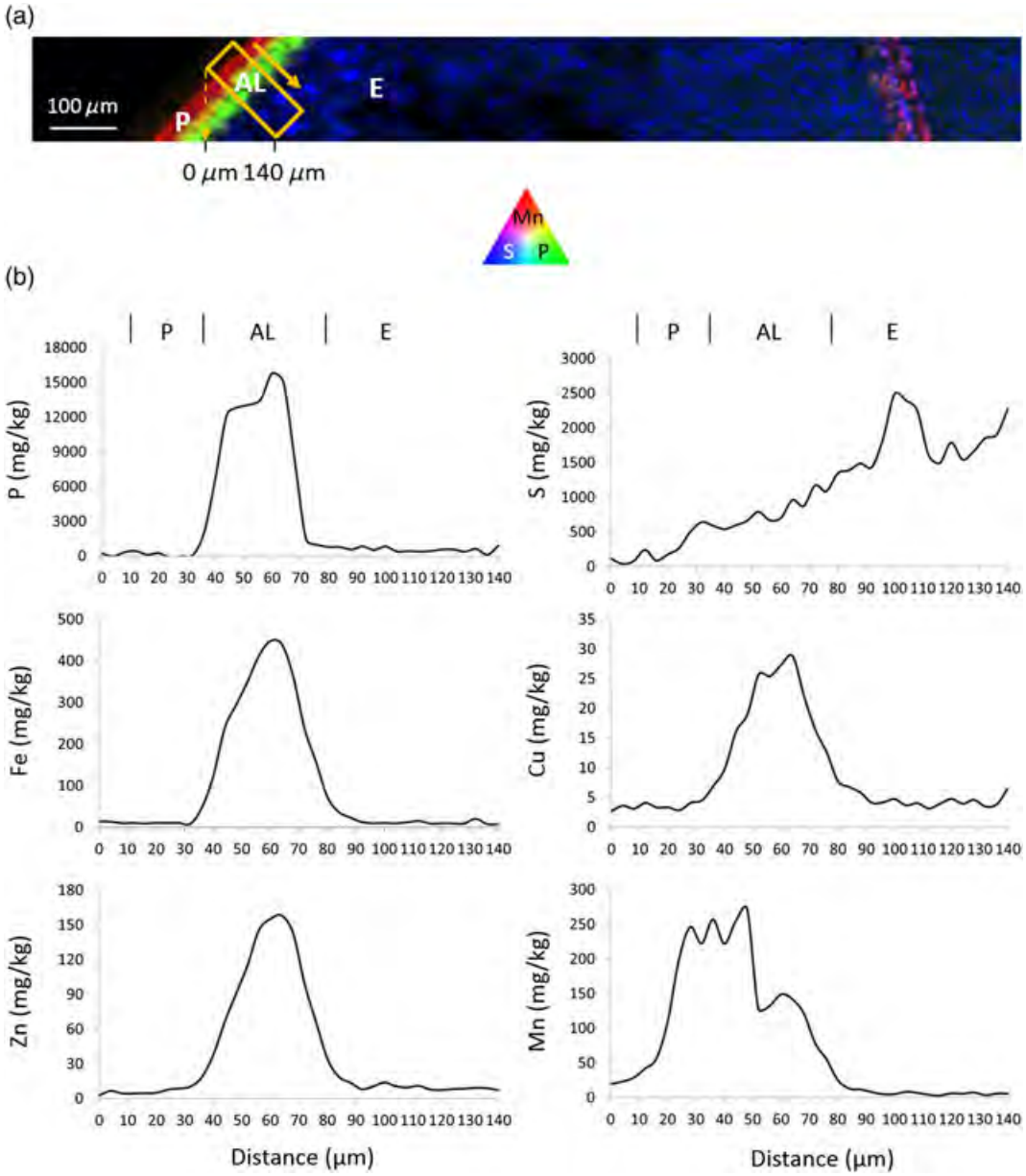

Figure 3. X-ray fluorescence microscopy of the mature wheat grain. Tri-colour map (A) of Mn (manganese; red), P (phosphorus; green) and S (sulfur; blue) distribution in the aleurone tissue. Element concentration profiles (B) of P, S, iron (Fe), Mn, copper (Cu) and zinc (Zn) from selected area (orange box). The data were obtained by using the transect function in GEOPIXE over an area 140 μm wide starting at the outer side. The letters in the figure and profiles indicate the pericarp (P), aleurone (AL) and endosperm (E).

30 and 75 μm from the outer side of the grain (Fig. 3B), which corresponds to the aleurone. In contrast, S is mainly present in the outer endosperm and only in small levels in the aleurone. The concentration of S in the endosperm is five times higher than that in the aleurone. Among all the elements investigated, Mn was most strongly localized in the outer parts of the grain (pericarp and testa) with the highest concentrations 20 to 50 μm from the edge of the grain. As Mn does not co-localize with P in the outermost bran tissues (10 to 40 μm), it is presumably not bound to phytate in the inner pericarp and testa. Cu, Fe and Zn were mainly localized in the same band (about 30 to 85 μm) which again corresponds to the aleurone layer. These cations co-localize with P and may be bound to phytate.

Crease region

Whilst Singh *et al.* (2014) observed large differences in element distribution in the crease tissues, higher resolution imaging coupled with speciation analysis are needed to better understand element translocation and accumulation. In the crease region (Fig. 2B), the individual cells of the nucellar projection and transfer cells are difficult to distinguish, whilst the cells in the modified aleurone (i.e. the aleurone surrounding the crease) can be clearly identified. Based on the element distribution, the different tissues in the crease region can be differentiated.

Figure 4B gives an overview of the concentrations of P, S, Fe, Cu, Mn and Zn in the crease region, computed from the averages of the vertical areas indicated by the box in the elemental map (Figs. 4A and S3). The large differences in concentrations between the endosperm and the crease tissues (Figs. 2 and 4B) indicate that physical and/or physiological barriers limit transport from the crease to the endosperm. These differ for the different elements because large gradients in concentrations of the elements are present in the crease region. P is below the detection limit in the nucellar projection (about 180 to 240 μm; Fig. 4B) but dominates in the modified aleurone cells (100 to 150 μm and 280 to 330 μm) in the crease. The concentration of P in the modified aleurone cells is about 50% of that in the aleurone cells, which implies that P is transported relatively efficiently to the aleurone cells. S concentration is highest in the nucellar projection. Slightly lower S concentrations were measured in the other parts of the crease. These concentrations were comparable to those in the aleurone and starchy endosperm (Fig. 4B). Fe and Cu are present in much higher concentrations in the nucellar projection than in the aleurone (Figs. 2B and 4B). Fe and P show distinctly different patterns, and these are in line with the results of Singh *et al.* (2014). These data suggest that Fe is not phytate-bound in this region. In contrast, Fe and S are distributed similarly. Singh *et al.* (2013) suggested that Fe may be bound to S-rich protein in the nucellar projection. Zn distribution is partially associated with P. The modified aleurone cells contain high levels of Zn, whereas Zn is below the detection limit in the nucellar projection. In contrast, the concentration of Zn in the modified aleurone cells is about four times higher than in the aleurone cells. Zn is also present in relatively high concentrations in the pigment strand situated between the nucellar epidermis and the modified aleurone cells. Our XFM results also show a high concentration of Zn in transfer cells (Fig. 2B). Tauris *et al.* (2009) found that many genes coding for Zn transporters in developing barley (*H. vulgare* L.) grains are present in the transfer cells. These transfer cells probably contain vacuoles in which Zn is stored before further transport occurs (Wang *et al.* 2011). Mn accumulates only in relatively low concentrations in the modified aleurone cells and is mainly present in the pigment strand.

Embryo tissue

Very few studies have investigated the distribution of elements in the wheat embryo; this is possibly a result of the spatial complexity of the embryo tissue and the lack of sensitivity of analytical methods. Lombi *et al.* (2009, 2011c) showed that XFM can reveal the spatial distribution of elements in rice and barley embryos with high sensitivity. In this study, the distribution of Mn, K, and Zn in the wheat embryo is mapped with high lateral resolution (2 μm, Figs. 5A and S4). Large elemental gradients are present in the embryo (Fig. 5A and Table 1). Zn is the predominant micronutrient in the shoot primordium, whereas the root primordium contains the highest concentrations of both Zn and Mn. Fe is largely absent in the root and shoot primordia, whilst the scutellum is rich in Fe and Mn (Fig. S5 and Table 1). This is in agreement with Mazzolini *et al.* (1985), who observed that the highest Mn level occurs in the outer perimeter of the root primordium, and that the scutellum is the main storage place for Fe accumulation (Mazzolini *et al.* 1985). However, the beam size used in their study did not yield high-resolution distribution maps for all elements investigated. Figure 5B shows the distribution of Zn, Mn and P in the wheat embryo tissues. P accumulates in the scutellum but is below the detection limit in the aleurone cells, the shoot and root primordia (Fig. 5B). In contrast, S occurs in the shoot and root primordia but not in the scutellum (Fig. 5C). Figure 5A–C was collected from the same longitudinal section. As Fe co-localizes with P, it is probably chelated by phytate. Zn and Mn are more prominently present in the shoot, particularly in the root primordium. They co-localize with S but not with P, which is low in these tissues. In barley grains, Zn is probably bound to the thiol groups of proteins and not chelated by phytate in the embryo (Persson *et al.* 2009).

The element distribution in the aleurone cells surrounding the embryo differs from that in the regular aleurone cells. The concentration of Zn in the former aleurone cells is twice as high as that of Fe (Table 1). Moreover, the highest concentration of Cu in the embryo tissue is in the aleurone cells.

In rice and barley, similar micronutrient distributions have been observed, with high Mn and Zn concentrations in the root primordium and Zn being the most abundant micronutrient in the shoot primordium (Takahashi *et al.* 2009; Lombi *et al.* 2011c). These results indicate that Mn and Zn have a similar abundance in the embryo. Zn and Mn are probably bound to S-containing amino acids (Persson *et al.* 2009). In meristematic

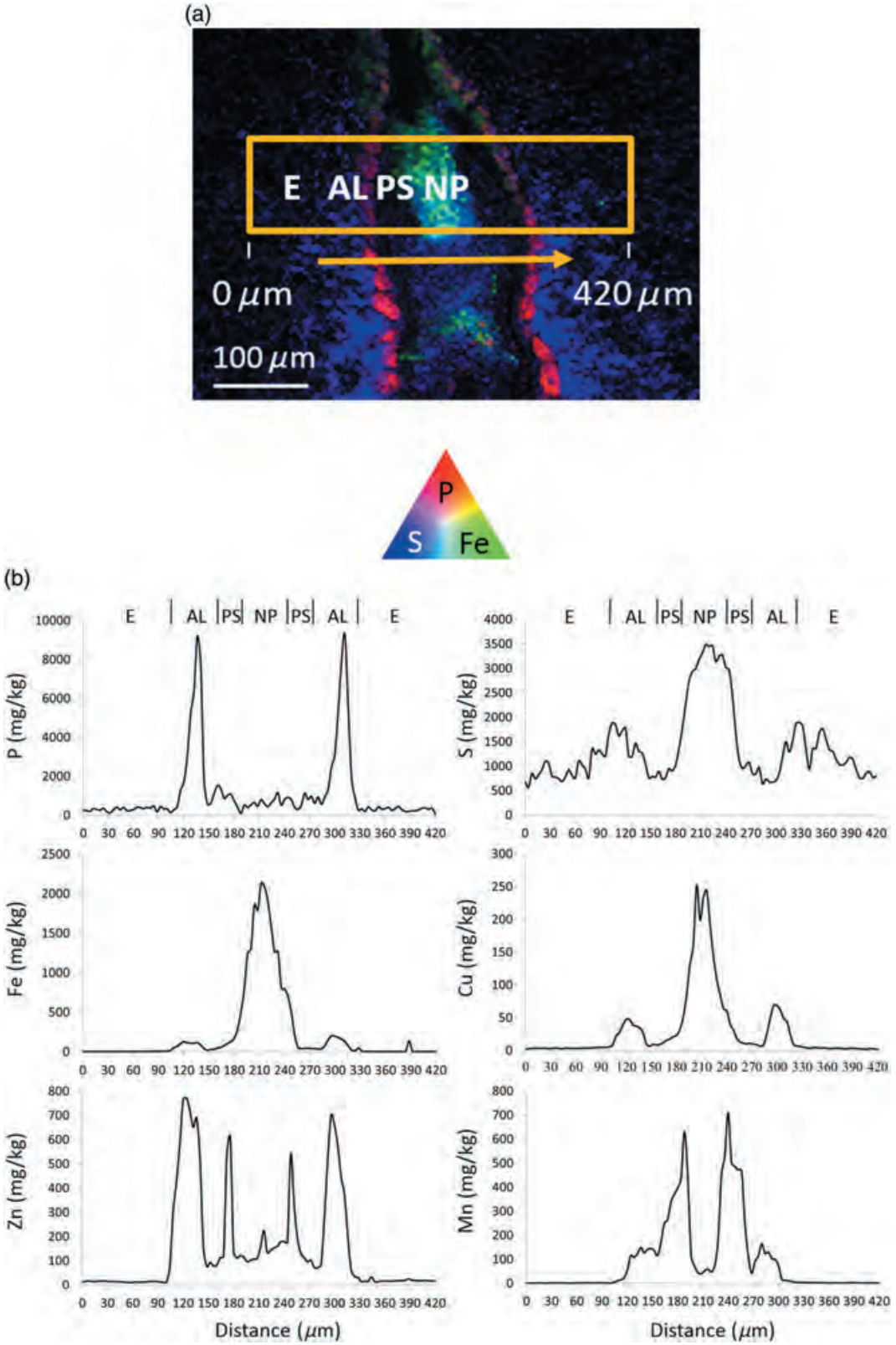

Figure 4. X-ray fluorescence microscopy of the mature wheat grain. Tri-colour map (A) of P (red), Fe (green), and S (blue) distribution in the crease region. Element concentration profiles (B) of P, S, Fe, Mn, Cu and Zn from selected area (orange box). The data were obtained by using the transect function in GEOPIXE over an area 420 μm wide. The letters in the figure and profiles indicate the individual cells of the endosperm (E), aleurone (AL), pigment strand (PS) and nucellar projection (NP).

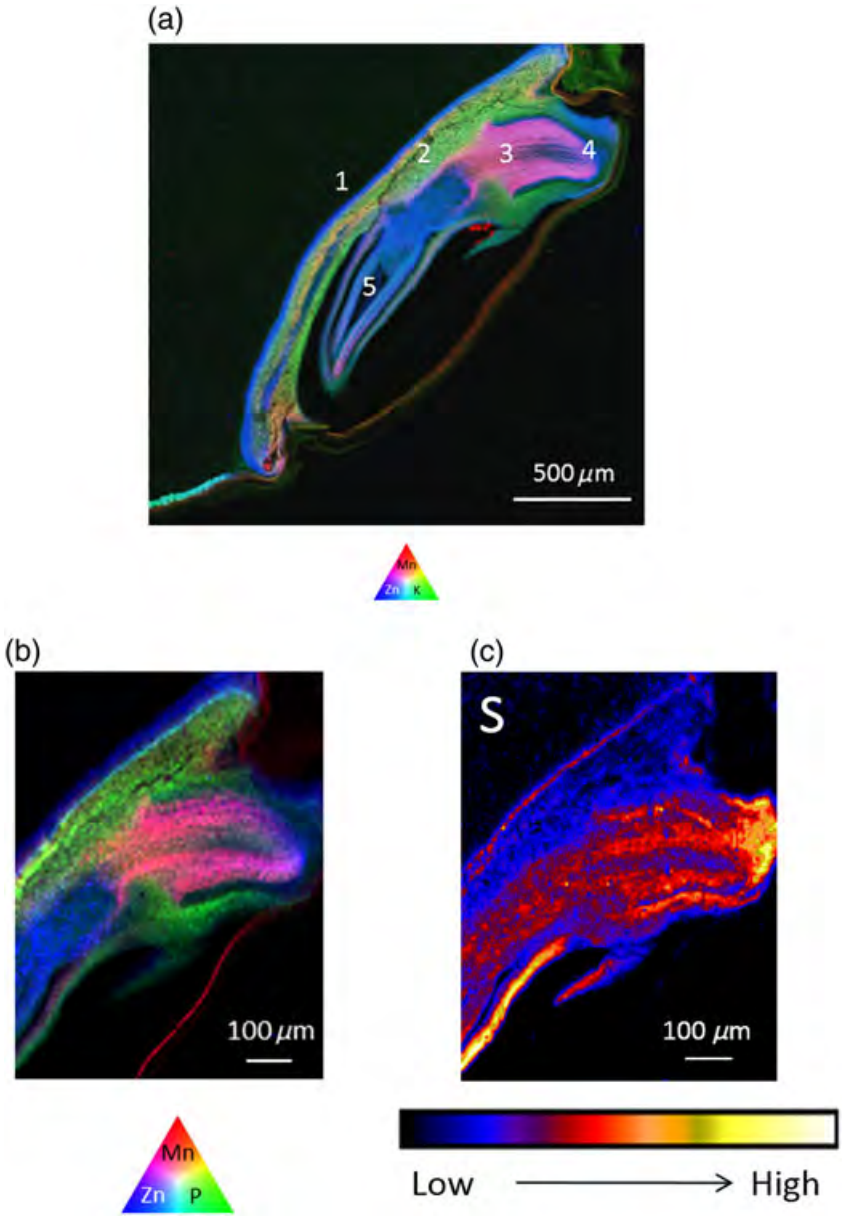

Figure 5. Tri-colour map (A) of Mn (red), K (potassium, green) and Zn (blue) distribution in a longitudinal section of the embryo and scutellum of a mature wheat grain with 1, aleurone; 2, scutellum; 3, radicula (root primordium); 4, calyptra (root cap); and 5, shoot primordium and with lateral resolution of 2 × 2 μm. Tri-colour map (B) of Mn (red), P (green) and Zn (blue) distribution in the embryo. X-ray fluorescence microscopy elemental map of S (C) present in the wheat embryo. The colour scale represents different concentrations, with black and white corresponding to the lowest and highest concentration, respectively.

tissues, Zn may play a role in protein synthesis and membrane structure (Cakmak 2008). Proteins in the embryos of maize, rice and wheat are mostly storage proteins, particularly 7S globulin (Shewry & Halford 2002).

Speciation of iron in the aleurone and crease regions using fluorescence-XANES imaging

Iron is present in plants as different chemical species. This influences its bioaccessibility and its nutritional value (Hurrell *et al.* 2004; Zheng *et al.* 2010). Determining the

Table 1. Concentrations (mg/kg) of Mn, Fe, Cu and Zn in the tissues of the wheat (*Triticum aestivum* L.) embryo

Element	Root primordium	Shoot primordium	Scutellum	Aleurone
Mn	562 (±103)	155 (±46)	288 (±32)	136 (±15)
Fe	182 (±20)	134 (±24)	275 (±51)	206 (±24)
Cu	25 (±2)	22 (±1)	28 (±2)	57 (±17)
Zn	271 (±30)	205 (±30)	110 (±24)	403 (±63)

Means and standard deviations of three analytical results of embryonic tissues of three independently sectioned wheat grains are given.

speciation of Fe within the different mature wheat grain tissues is therefore important. Based on the Fe K-edge XANES measurements on intact whole grains, Singh *et al.* (2013) suggested that about 80% of the Fe is present in ferric form, and the remainder is in ferrous form. However, these authors did not present any information at tissue level, and their XANES spectra have a high noise-to-signal ratio. In our study, the oxidation state of Fe and the type of Fe ligands (specific bonding environments) in different wheat tissues were studied using XANES (Fig. S6). Each different Fe species is characterized by a different Fe K-edge XANES spectrum (Fig. 6 – spectra of standards). In general, for the ferric compounds, the principal peak (white line) of the Fe K-edge is about 2.5 to 3.0 eV higher than for the ferrous compounds (i.e. a shift from about 7129 to 7132 eV). Furthermore, both ferrous and ferric phytates exhibit a shoulder feature at 7135 eV. In addition, the energy position of the inflection point of the absorption edge (the maximum point of the first derivative of the K-edge spectrum) increases from about 7122 to 7128 eV with increasing average Fe oxidation state which is in agreement with Prietzel *et al.* (2007). Figure 6 shows that the XANES spectra of Fe differ between the aleurone cells, modified aleurone cells and nucellar projection. The XANES spectrum of the aleurone cells has an inflection point at 7123 eV, a principal peak at about 7130 eV (Table S1) and a shoulder at higher energies. This suggests that ferrous Fe-phytate occurs in the aleurone cells. The shoulder at higher energies is also present in the spectrum of the modified aleurone cells, but the lower-energy feature is less prominent than it is for the aleurone cells. The modified aleurone cells have a Fe K-edge at 7131 eV and an inflection point at 7126 eV (Table S1), indicating that both ferrous and ferric Fe-phytates co-occur. In the nucellar projection, the principal Fe K-edge peak is at 7132 eV, and the inflection point of the absorption edge is at 7126 eV, indicating the presence of ferric Fe (Table S1). The shoulder at higher energies, observed in both the aleurone and modified aleurone cells spectra, is absent in this Fe-spectrum, possibly suggesting that it does not contain Fe-phytate.

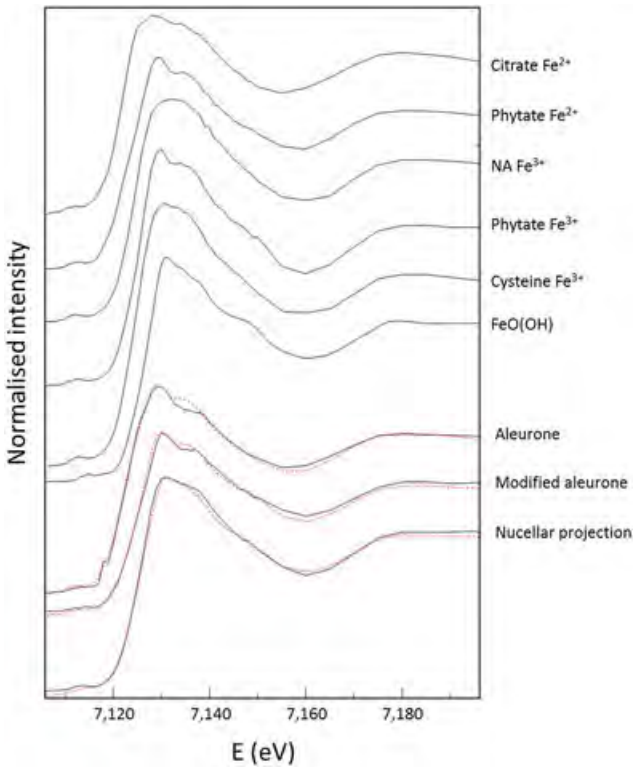

Figure 6. Fe X-ray absorption near-edge spectroscopy spectra from reference Fe compound standards [citrate Fe^{2+}, phytate Fe^{2+}, nicotianamine (NA) Fe^{3+}, phytate Fe^{3+}, cysteine Fe^{3+}, FeO(OH)] and cross mature wheat grain sections. The dotted lines give the linear combination fitting results.

To further unravel the speciation of Fe, the Fe-XANES spectra of the grains were analysed by LCF using the XANES spectra of standard compounds. Figure 6 only shows the relevant standards (cf. infra). The linear combination fitting analysis can be used to indicate the relative amount of major species in the samples. On the basis of this analysis, two-thirds of the Fe in the aleurone cells was assigned to phytate Fe^{2+} (0.67 ± 0.01) and one-third to citrate or citrate-like Fe^{2+} (0.33 ± 0.01), whilst the modified aleurone cells were indicated to contain almost equal contributions of phytate Fe^{3+} (0.57 ± 0.02) and phytate Fe^{2+} (0.43 ± 0.02). These contributions (± standard deviations) of each standard spectrum to the fit are based on spectra of at least four different regions (Fig. S6). In the aleurone cells, Fe is mainly chelated not only by phytate but also by citrate (or citrate-like ligands). In the modified aleurone cells, LCF indicates that both ferrous and ferric Fe are chelated by phytate, and this is reflected in the co-occurrence of Fe and P in these tissues (cf. supra). During transport from the modified aleurone cells to the aleurone cells or starchy endosperm, Fe is probably chelated by citrate. Although we incorporated the major Fe species occurring in plant material as standards for the LCF analysis, the small feature after the white line in the fitted curves of aleurone and modified aleurone, which is not present in the experimental data, indicated that another Fe species may occur in these tissues. The LCF analysis showed that the best fit was obtained for a combination of citrate Fe^{2+} (0.08), NA Fe^{3+} (0.24) and FeO(OH) (0.68) in the nucellar projection. The XANES spectrum of the nucellar projection was extracted from one area (Fig. S6). Because of the poor solubility of Fe ions, translocation inside the plant occurs with chelating molecules like citrate, NA and deoxymugineic acid (Bashir *et al.* 2010; Kobayashi & Nishizawa 2012). In the phloem, Fe is probably chelated to NA during transport (Briat *et al.* 2007). The LCF results show that Fe is not only bound to organic chelators in the nucellar projection but may also contain more complex Fe species (possibly inorganic). This is in contrast to the aleurone, which is the principal element-storage region of the mature grain. Although S and Fe co-localize in the nucellar projection, our LCF results indicate that Fe is probably not bound to cysteine in this tissue. Our results for the nucellar projection should be carefully interpreted because the chemical structure of the chelating molecules could not be unequivocally identified.

Table 2. Overview of the concentration (mg/kg) and speciation of Fe in the tissues of the wheat (*Triticum aestivum* L.) aleurone, embryo and crease region

Tissue		Concentration (mg/kg)	Ligand
Aleurone		366 (±37)	Phytate/citrate[a]
Embryo	Scutellum	275 (±51)	*Phytate*[b]
	Root primordium	182 (±20)	*Protein*[b]
	Shoot primordium	134 (±24)	*Protein*[b]
Crease region	Nucellar projection	1895 (—)	Fe-NA/FeO(OH)[a]
	Pigment strand	66 (±24)	nd
	Modified aleurone	306 (±24)	Phytate[a]

Means and standard deviations of at least three analytical results are given.
nd: not determined
[a]Derived from XANES imaging.
[b]Derived from co-localization of Fe with its possible ligands.

CONCLUSIONS

In conclusion, this study imaged the gradients in elemental distribution in detail among bran tissues, crease region and embryo. Table 2 summarizes the distribution and speciation of Fe throughout these tissues. Of all the elements studied, Mn is mainly concentrated in the testa. The other elements are mostly localized in the aleurone. Strong similarities were observed in the distribution of Fe and Zn and P in the bran tissues, indicating that Fe and Zn are confined to the spherical phytate globoids in the aleurone, and this is in line with the XANES Fe speciation results. Phytates serve as a source of P for the synthesis of membrane lipids and nucleic acids for the grain during germination and also functions as storage sites for divalent elements such as magnesium, Ca, Fe and Zn, thereby acting as major cation traps for eliminating excessive cellular concentrations of these elements (Hawkesford *et al*. 2012). The chelation of Fe by phytate suppresses Fe-catalysed oxidative reactions and, hence, the generation of cellular free radicals which are extremely toxic to plants. Thus, phytate structures preserve the viability of the seed as potent antioxidants during dormancy (Graf & Eaton 1990; Takahashi *et al*. 2009). In the crease region, Mn and Zn are present in the pigment strand, but the highest concentrations of Zn occur in the modified aleurone cells. In contrast, Fe and Cu predominantly occur in the nucellar projection and are not co-located with P. Elements enter the wheat grain during maturation through the different tissues of the crease region. Our results show the various barriers which limit elemental transport in wheat grain tissues. Fe is chelated by phytate in the modified aleurone cells but not in the nucellar projection. Because most cation-phytate chelates are highly insoluble at the pH of a plant cell, Fe is most probably chelated by small molecules such as NA during transport from the plant to the grain. Therefore, Fe is not chelated by phytate in the vascular tissues. Large elemental gradients are also present in the embryo. Fe co-localizes with P in the scutellum, whilst Zn and Mn are primarily present in the shoot and especially root primordium, probably bound to thiol groups of proteins. In such highly metabolically active root and shoot tissues, during germination, Zn ions are most probably used for protein synthesis, membrane function, cell elongation and tolerance to environmental stress. These results are relevant to further research investigating ways to enhance the bioaccessibility of nutrient elements by plant breeding, biofortification and/or processing. Moreover, the results form a knowledge platform for identifying transporters and chelating compounds that may be involved in transport and deposition of nutrient elements in the wheat grain.

ACKNOWLEDGMENTS

This research was conducted in the framework of the W. K. Kellogg Chair in Cereal Science and Nutrition at the KU Leuven (chair holders J. A. Delcour and K. Verbeke), is part of Methusalem programme 'Food for the Future' (2007–2021) and was undertaken on the X-ray fluorescence microscopy beamline at the Australian Synchrotron, Victoria, Australia. We gratefully acknowledge the 'Fonds voor Wetenschappelijk Onderzoek Vlaanderen' (FWO, Brussels, Belgium) for the travel grant for the stay abroad to Niels De Brier. Fruitful discussions with Drs. C.M. Courtin (KU Leuven), L. Sanders, K. Spence, J. Reid, A. Birkett, N. Almeida and R. McDermott (Kellogg Company, Battle Creek, Michigan, USA) are highly appreciated.

REFERENCES

Barron C., Surget A. & Rouau X. (2007) Relative amounts of tissues in mature wheat (*Triticum aestivum* L.) grain and their carbohydrate and phenolic acid composition. *Journal of Cereal Science* **45**, 88–96.

Bashir K., Ishimaru Y. & Nishizawa N.K. (2010) Iron uptake and loading into rice grains. *Rice* **3**, 122–130.

Baynes R. & Bothwell T. (1990) Iron deficiency. *Annual Review of Nutrition* **10**, 133–148.

Bechtel D.B., Abécassis J., Shewry P.R. & Evers A.D. (2009) Development, structure, and mechanical properties of the wheat grain. In *Wheat Chemistry and Technology* (eds Khan K. & Shewry P.R.) 4th edn. AACC International, St. Paul, MN, USA.

Borg S., Brinch-Pedersen H., Tauris B. & Holm P.B. (2009) Iron transport, deposition and bioavailability in the wheat and barley grain. *Plant and Soil* **325**, 15–24.

Bradbury D., MacMasters M.M. & Cull I.M. (1956a) Structure of the mature wheat kernel IV. Microscopic structure of the germ of hard red winter wheat. *Cereal Chemistry* **33**, 373–394.

Bradbury D., MacMasters M.M. & Cull I.M. (1956b) Structure of the mature wheat kernel. II. Microscopic structure of pericarp, seed coat, and other coverings of the endosperm and the germ of hard red winter wheat. *Cereal Chemistry* **33**, 342–360.

Bradbury D., MacMasters M.M. & Cull I.M. (1956c) Structure of the mature wheat kernel. III. Microscopic structure of the endosperm of hard red winter wheat. *Cereal Chemistry* **33**, 361–373.

Briat J.-F., Curie C. & Gaymard F. (2007) Iron utilization and metabolism in plants. *Current Opinion in Plant Biology* **10**, 276–282.

Brouns F., Hemery Y., Price R. & Anson N.M. (2012) Wheat aleurone: separation, composition, health aspects, and potential food use. *Critical Reviews in Food Science and Nutrition* **52**, 553–568.

Brown K.H., Peerson J.M., Baker S.K. & Hess S.Y. (2009) Preventive zinc supplementation among infants, preschoolers, and older prepubertal children. *Food Nutritional Bulletin* **30**, S12–S40.

Cakmak I. (2008) Enrichment of cereal grains with zinc: agronomic or genetic biofortification? *Plant and Soil* **302**, 1–17.

Cakmak I., Pfeiffer W.H. & McClafferty B. (2010) Review: biofortification of durum wheat with zinc and iron. *Cereal Chemistry* **87**, 10–20.

De Brier N., Gomand S.V., Donner E., Paterson D., Delcour J.A., Lombi E. & Smolders E. (2015) Distribution of minerals in wheat grains (*Triticum aestivum* L.) and in roller milling fractions affected by pearling. *Journal of Agricultural and Food Chemistry* **63**, 1276–1285.

Delcour J.A. & Hoseney R.C. (2010) *Principles of Cereal Science and Technology*3rd edn. AACC International, St. Paul, MN, USA.

Dornez E., Holopainen U., Cuyvers S., Poutanen K., Delcour J.A., Courtin C.M. & Nordlund E. (2011) Study of grain cell wall structures by microscopic analysis with four different staining techniques. *Journal of Cereal Science* **54**, 363–373.

Dubois M., Geddes W.F. & Smith F. (1960) The carbohydrates of the Gramineae. X. A quantitative study of the carbohydrates of wheat germ. *Cereal Chemistry* **37**, 557–567.

Eagling T., Neal A.L., McGrath S.P., Fairweather-Tait S., Shewry P.R. & Zhao F.-J. (2014) Distribution and speciation of iron and zinc in grain of two wheat genotypes. *Journal of Agricultural and Food Chemistry* **62**, 708–716.

Ebel H., Svagera R., Ebel M.F., Shaltout A. & Hubbell J.H. (2003) Numerical description of photoelectric absorption coefficients for fundamental parameter programs. *X-Ray Spectrometry* **32**, 442–451.

Eeckhout W. & De Paepe M. (1994) Total phosphorus, phytate–phosphorus and phytase activity in plant feedstuffs. *Animal Feed Science and Technology* **47**, 19–29.

Elam W.T., Ravel B.D. & Sieber J.R. (2002) A new atomic database for X-ray spectroscopic calculations. *Radiation Physics and Chemistry* **63**, 121–128.

Etschmann B.E., Donner E., Brugger J., Howard D.L., de Jonge M.D., Paterson D., … Lombi E. (2014) Speciation mapping of environmental samples using XANES imaging. *Environmental Chemistry* **11**, 341–350.

Evers T. & Millar S. (2002) Cereal grain structure and development: some implications for quality. *Journal of Cereal Science* **36**, 261–284.

Graf E. & Eaton J.W. (1990) Antioxidant functions of phytic acid. *Free Radical Biology and Medicine* **8**, 61–69.

Grafe M., Donner E., Collins R.N. & Lombi E. (2014) Speciation of metal(loid)s in environmental samples by X-ray absorption spectroscopy: a critical review. *Analytica Chimica Acta* **822**, 1–22.

Graham R.D., Welch R.M., Saunders D.A., Ortiz-Monasterio I., Bouis H.E., Bonierbale M., … Twomlow S. (2007) Nutritious subsistence food systems. *Advances in Agronomy*, **92** 1–74.

Hawkesford M., Horst W., Kichey T., Lambers H., Schjoerring J.K., Skrumsager I. & White P.J. (2012) Functions of macronutrients. In *Mineral Nutrition of Higher Plants* (ed Marschner P.) 3rd edn, pp. 135–189. Elsevier, London, UK.

Hurrell R.F., Lynch S., Bothwell T., Cori H., Glahn R., Hertrampf E., … Zimmermann M.B. (2004) Enhancing the absorption of fortification iron. *International Journal for Vitamin and Nutrition Research* **74**, 387–401.

Jacobsen T. & Slotfeldt-Ellingsen K.D. (1983) Phytic acid and metal availability: a study of Ca and Cu binding foodstuffs. *Cereal Chemistry* **60**, 392–395.

Kobayashi T. & Nishizawa N.K. (2012) Iron uptake, translocation, and regulation in higher plants. *Annual Review of Plant Biology* **63**, 131–152.

Kopittke P.M., de Jonge M.D., Wang P., McKenna B.A., Lombi E., Paterson D.J., … Menzies N.W. (2014) Laterally resolved speciation of arsenic in roots of wheat and rice using fluorescence-XANES imaging. *New Phytologist* **201**, 1251–1262.

Lee S., Persson D.P., Hansen T.H., Husted S., Schjoerring J.K., Kim Y.-S., … An G. (2011) Bio-available zinc in rice seeds is increased by activation tagging of nicotianamine synthase. *Plant Biotechnology Journal* **9**, 865–873.

Li H.F., Lombi E., Stroud J.L., McGrath S.P., & Zhao F.J. (2010) Selenium speciation in soil and rice: influence of water management and Se fertilization. *Journal of Agricultural and Food Chemistry* **58**, 11837–11843.

Liu Z.H., Wang H.Y., Wang X.E., Xu H., Gao D., Zhang G.P., … Liu D.J. (2008) Effect of wheat pearling on flour phytase activity, phytic acid, iron, and zinc content. *LWT — Food Science and Technology* **41**, 521–527.

Lombi E., de Jonge M.D., Donner E., Ryan C.G. & Paterson D. (2011a) Trends in hard X-ray fluorescence mapping: environmental applications in the age of fast detectors. *Analytical and Bioanalytical Chemistry* **400**, 1637–1644.

Lombi E., Scheckel K.G. & Kempson I.M. (2011b) *In situ* analysis of metal(loid)s in plants: state of the art and artefacts. *Environmental and Experimental Botany* **72**, 3–17.

Lombi E., Scheckel K.G., Pallon J., Carey A.M., Zhu Y.G. & Meharg A.A. (2009) Speciation and distribution of arsenic and localization of nutrients in rice grains. *New Phytologist* **184**, 193–201.

Lombi E., Smith E., Hansen T.H., Paterson D., de Jonge M.D., Howard D.L., … Schjoerring J.K. (2011c) Megapixel imaging of (micro)nutrients in mature barley grains. *Journal of Experimental Botany* **62**, 273–282.

Lopez H.W., Leenhardt F., Coudray C. & Remesy C. (2002) Minerals and phytic acid interactions: is it a real problem for human nutrition? *International Journal of Food Science & Technology* **37**, 727–739.

Lott J.N.A., Randall P.J., Goodchild D.J. & Craig S. (1985) Occurrence of globoid crystals in cotyledonary protein bodies of *Pisum sativum* as influenced by experimentally induced changes in Mg, Ca and K contents of seeds. *Australian Journal of Plant Physiology* **12**, 341–353.

Mazzolini A.P., Pallaghy C.K. & Legge G.J.F. (1985) Quantitative microanalysis of Mn, Zn and other elements in mature wheat seed. *New Phytologist* **100**, 483–509.

Moore K.L., Zhao F.-J., Gritsch C.S., Tosi P., Hawkesford M.J., McGrath S.P., … Grovenor C.R.M. (2012) Localisation of iron in wheat grain using high resolution secondary ion mass spectrometry. *Journal of Cereal Science* **55**, 183–187.

Morrison I.N., Kuo J. & O'Brien T.P. (1975) Histochemistry and fine structure of developing wheat aleurone cells. *Planta* **123**, 105–116.

Neal A.L., Geraki K., Borg S., Quinn P., Mosselmans J.F., Brinch-Pedersen H. & Shewry P.R. (2013) Iron and zinc complexation in wild-type and ferritin-expressing wheat grain: implications for mineral transport into developing grain. *Journal Biological Inorganic Chemistry* **18**, 557–570.

O'Brien T.P., Sammut M.E., Lee J.W., & Smart M.G., (1985) The vascular system of the wheat spikelet. *Functional Plant Biology* **12**, 487–511.

Paterson D., de Jonge M.D., Howard D.L., Lewis W., McKinlay J., Starritt A., … Siddons D.P. (2011) The X-ray fluorescence microscopy beamline at the Australian synchrotron. *AIP Conference Proceedings* **1365**, 219–222.

Pearson J.N., Rengel Z., Jenner C.F. & Graham R.D. (1995) Transport of zinc and manganese to developing wheat grains. *Physiologia Plantarum* **95**, 449–455.

Persson D.P., Hansen T.H., Laursen K.H., Schjoerring J.K. & Husted S. (2009) Simultaneous iron, zinc, sulfur and phosphorus speciation analysis of barley grain tissues using SEC-ICP-MS and IP-ICP-MS. *Metallomics* **1**, 418–426.

Pfeiffer W.H. & McClafferty B. (2007) HarvestPlus: breeding crops for better nutrition. *Crop Science* **47**, S88–S105.

Piironen V., Lampi A.-M., Ekholm P., Salmenkallio-Martilla M. & Liukkonen K.-H. (2009) Micronutrients and phytochemicals in wheat grain. In *Wheat Chemistry and Technology* (eds Khan K. & Shewry P.R.) 4th edn. AACC International, St. Paul, MN, USA.

Prasad A.S. (2009) Zinc: role in immunity, oxidative stress and chronic inflammation. *Current Opinion in Clinical Nutrition & Metabolic Care* **12**, 646–652.

Prietzel J., Thieme J., Eusterheus K. & Eichert D. (2007) Iron speciation in soils and soil aggregates by synchrotron-based X-ray microspectroscopy (XANES, μ-XANES). *European Journal of Soil Science* **58**, 1027–1041.

Ravel B. & Newville M. (2005) ATHENA, ARTEMIS, HEPHAESTUS: data analysis for X-ray absorption spectroscopy using IFEFFIT. *Journal of Synchrotron Radiation* **12**, 537–541.

Rengel Z., Batten G.D. & Crowley D.E. (1999) Agronomic approaches for improving the micronutrient density in edible portions of field crops. *Field Crops Research* **60**, 27–40.

Ryan C.G. (2000) Quantitative trace elements imaging using PIXE and the nuclear microprobe. *International Journal of Imaging Systems and Technology* **11**, 219–230.

Ryan C.G., Etschmann B.E., Vogt S., Maser J., Harland C.L., van Achterbergh E. & Legnini D. (2005) Nuclear microprobe — synchrotron synergy: towards integrated quantitative real-time elemental imaging using PIXE and SXRF. *Nuclear Instruments and Methods in Physics Research Section B: Beam Interactions with Materials and Atoms* **231**, 183–188.

Shetlar M.R., Rankin G.T., Lyman J.F. & France W.G. (1947) Investigation of the proximate chemical composition of the separate bran layers of wheat. *Cereal Chemistry* **24**, 111–122.

Shewry P.R. & Halford N.G. (2002) Cereal seed storage proteins: structures, properties and role in grain utilization. *Journal of Experimental Botany* **53**, 947–958.
Singh S.P., Vogel-Mikuš K., Arčon I., Vavpetič P., Jeromel L., Pelicon P., … Tuli R. (2013) Pattern of iron distribution in maternal and filial tissues in wheat grains with contrasting levels of iron. *Journal of Experimental Botany* **64**, 3249–3260.
Singh S.P., Vogel-Mikus K., Vavpetic P., Jeromel L., Pelicon P., Kumar J. & Tuli R. (2014) Spatial X-ray fluorescence micro-imaging of minerals in grain tissues of wheat and related genotypes. *Planta* **240**, 277–289.
Takahashi M., Nozoye T., Kitajima N., Fukuda N., Hokura A., Terada Y., … Nishizawa N.K. (2009) *In vivo* analysis of metal distribution and expression of metal transporters in rice seed during germination process by microarray and X-ray fluorescence imaging of Fe, Zn, Mn, and Cu. *Plant and Soil* **325**, 39–51.
Tanaka K., Yoshida T. & Kasai Z. (1974) Distribution of mineral elements in the outer layer of rice and wheat grains, using electron microprobe X-Ray analysis. *Soil Science and Plant Nutrition* **20**, 87–91.
Tang J., Zou C., He Z., Shi R., Ortiz-Monasterio I., Qu Y. & Zhang Y. (2008) Mineral element distributions in milling fractions of Chinese wheats. *Journal of Cereal Science* **48**, 821–828.
Tauris B., Borg S., Gregersen P.L. & Holm P.B. (2009) A roadmap for zinc trafficking in the developing barley grain based on laser capture microdissection and gene expression profiling. *Journal of Experimental Botany* **60**, 1333–1347.
Wang P., Menzies N.W., Lombi E., McKenna B.A., James S., Tang C. & Kopittke P.M. (2015) Synchrotron-based X-ray absorption near-edge spectroscopy imaging for laterally resolved speciation of selenium in fresh roots and leaves of wheat and rice. *Journal of Experimental Botany* . DOI:10.1093/jxb/erv254.
Wang Y.X., Specht A. & Horst W.J. (2011) Stable isotope labelling and zinc distribution in grains studied by laser ablation ICP-MS in an ear culture system reveals zinc transport barriers during grain filling in wheat. *New Phytologist* **189**, 428–437.
Weekley C.M., Aitken J.B., Finney L., Vogt S., Witting P.K. & Harris H.H. (2013) Selenium metabolism in cancer cells: the combined application of XAS and XFM techniques to the problem of selenium speciation in biological systems. *Nutrients* **5**, 1734–1756.
Wessells K.R. & Brown K.H. (2012) Estimating the global prevalence of zinc deficiency: results based on zinc availability in national food supplies and the prevalence of stunting. *PLoS ONE* **7**, e50568.
White P.J. (2012) Long-distance transport in the xylem and phloem. In *Mineral Nutrition of Higher Plants* (ed Marschner P.) 3rd edn, pp. 49–70. Elsevier, London, UK.
WHO (2008) Worldwide prevalence of anaemia 1993-2005. *WHO Global Database on Anaemia*. WHO Press, Geneva, Switzerland.
WHO (2015) *The global prevalence of anaemia in 2011*. WHO Press, Geneva, Switzerland.
Xue Y.-F., Eagling T., He J., Zou C.-Q., McGrath S.P., Shewry P.R. & Zhao F.-J. (2014) Effects of nitrogen on the distribution and chemical speciation of iron and zinc in pearling fractions of wheat grain. *Journal of Agricultural and Food Chemistry* **62**, 4738–4746.
Zheng L., Cheng Z., Ai C., Jiang X., Bei X., Zheng Y., … Shou H. (2010) Nicotianamine, a novel enhancer of rice iron bioavailability to humans. *PLoS ONE* **5**, e10190.

Received 26 August 2015; received in revised form 17 March 2016; accepted for publication 24 March 2016

SUPPORTING INFORMATION

Additional Supporting Information may be found in the online version of this article at the publisher's web-site:

Table S1. Energy positions of the inflection point of the absorption edge and the white line of Iron (Fe) K-edge X-ray absorption near-edge spectroscopy spectra acquired for different reference Fe-compound standards and wheat grain tissues.
Figure S1. Fe map of a wheat grain bisected transversely in a central plane with a lateral resolution of 4×4 μm. The colour scale represents different concentrations, with black and white corresponding to the lowest and highest concentrations, respectively.
Figure S2. Elemental maps of a wheat grain bisected transversely in a central plane with focus on aleurone tissue with a lateral resolution of 1×2 μm. The colour scale represents different concentrations, with black and white corresponding to the lowest and highest concentrations, respectively.
Figure S3. Elemental maps of a wheat grain bisected transversely in a central plane with focus on crease region with a lateral resolution of 1×2 μm. The colour scale represents different concentrations, with black and white corresponding to the lowest and highest concentration, respectively.
Figure S4. Tri-colour map of Mn (red), K (green) and Zn (blue) distribution in a longitudinal section of the embryo and scutellum of a mature wheat grain.
Figure S5. Fe map of longitudinal section of wheat embryo with a lateral resolution of 2×2 μm. The colour scale represents different concentrations, with black and white corresponding to the lowest and highest concentration, respectively.
Figure S6. Fe maps of a wheat grain bisected transversely in a central plane with a lateral resolution of 2×2 μm. The regions of (A) aleurone cells, (B) modified aleurone cells and (C) nucellar projection that were selected for extraction of the X-ray absorption near-edge spectroscopy spectra are indicated by the green shapes. The colour scale represents different concentrations, with black and white corresponding to the lowest and highest concentration, respectively.